Tunable Elasto-Viscoplastic Properties of Polymer Blends for 3D Printing Applications

N.B. When citing this work, cite the original published paper.

(article starts on next page)

RESEARCH ARTICLE OPEN ACCESS

Tunable Elasto-Viscoplastic Properties of Polymer Blends for 3D Printing Applications

Ases Akas Mishra[1] 🆔 | Manoj Chandregowda[2] | Janina Faiß[3] | Marko Bek[1,4] | Ann E. Terry[5,4] | Kim Nygård[5,4] | Dragana Arlov[6,4] | Roland Kádár[1,5,4]

[1]Chalmers University of Technology, Department of Industrial and Materials Science, Göteborg, Sweden | [2]Chalmers University of Technology, Department of Chemistry and Chemical Engineering, Göteborg, Sweden | [3]University of Stuttgart, Chemical- and Bio-Engineering, Stuttgart, Germany | [4]LINXS Institute of advanced Neutron and X-ray Science (LINXS), Lund, Sweden | [5]Lund University, MAX IV Laboratory, Lund, Sweden | [6]Tetra Pak Processing Systems, Lund, Sweden

Correspondence: Ases Akas Mishra (ases@chalmers.se) | Roland Kádár (roland.kadar@chalmers.se)

Received: 14 March 2025 | **Revised:** 9 May 2025

Funding: This project has received funding from the European Union's Horizon 2020 research and innovation programme under the Marie Skłodowska-Curie grant agreement No 955605.

Keywords: 3D printing | die swelling | elasto-viscoplastic | inkjet printing | viscoelasticity | yield stress

ABSTRACT

Post-extrusion flow dynamics of soft matter are governed by their elasto-viscoplastic (EVP) rheological properties, which influence filament stability, die swelling, and shape fidelity in extrusion-based 3D printing. Achieving precision and control in printed structures requires optimizing yield stress, viscoelasticity, and extrusion pressure to minimize excessive die swelling and material spreading, which can lead to unstable extrusion and poor print fidelity. We investigate Carbopol-polyethylene oxide (PEO) blends as model EVP fluids, systematically varying their composition to assess die swelling, print width, and deposition accuracy. Rheo-SAXS measurements reveal that die swelling can be directly related to characteristic nanoscale lengthscales. Parametric analysis using the Ohnesorge (Oh) and modified Bingham (ξ/Bi) numbers reveals that at high ξ/Bi (yield stress, $\sigma_y < 1$ Pa) and $Oh < 0.1$, surface tension and viscoelastic effects dominate, leading to excessive die swelling and spreading upon deposition (up to 1.6 and 6 times the nozzle diameter, respectively), ultimately causing drop formation rather than stable filament extrusion. Conversely, $Oh \geq 10^2$ and $\xi/Bi \leq 8 \times 10^4$ ensure optimal printability, high shape fidelity, and minimal die swelling. These findings guide EVP formulation and optimal extrusion pressure using dimensionless groups that capture material rheology and flow behavior.

1 | Introduction

Elasto-viscoplastic (EVP) fluids exhibit a combination of viscoelastic and viscoplastic behavior, imparting unique flow characteristics that are essential in a range of industrial applications. These fluids are widely used in inkjet [1] and 3D printing [2] due to their tunable rheological properties, which can be controlled by adjusting concentration and composition. The ability to manipulate yield stress, shear-thinning behavior, and viscoelasticity makes them ideal candidates for extrusion-based

manufacturing and printing processes. In the extrusion of EVP fluids, yield stress ensures that the material remains inside the nozzle without dripping [3]. Shear thinning facilitates extrusion by reducing viscosity under applied shear, allowing controlled extrusion and deposition [4]. Viscoelasticity introduces elastic recovery, making the material suitable for droplet formation in inkjet printing [5]. Finally, yield stress plays a crucial role in ensuring the printed material holds its shape post-deposition, preventing excessive spreading or collapse [3]. Given the importance of these rheological properties, their precise

control is essential for optimizing performance in various applications.

To achieve desirable EVP characteristics, the blending of non-Newtonian fluids has been increasingly explored [6, 7]. By carefully optimizing their compositions, tailored materials with enhanced yield stress, shear-thinning, and viscoelastic properties can be developed. Examples include xanthan gum-cellulose blends for food thickeners [8], gelatin-guar gum-polyvinyl alcohol (PVA) for biomedical applications [9], and polyacrylamide-sodium alginate for controlled drug delivery [10, 11].

Carbopol, a widely used rheology modifier, is a cross-linked polymer of acrylic acid commonly employed to enhance the rheological properties of various materials [12]. It finds applications in personal care products, pharmaceuticals, and food industries, where it improves texture, stability, and controlled release. When dispersed in water and neutralized with a base, Carbopol forms a microgel structure that imparts yield stress and viscoelastic characteristics to the material [13, 14]. PEO is a high molecular weight, linear chain polymer that can be used to significantly enhance the viscoelastic properties of materials [15]. Carbopol-PEO blends form structurally [16] and thermally [17] stable interpolymer complexes via hydrogen bonding, influenced by factors like salt concentration and pH. The blending of Carbopol with PEO has been shown to enhance EVP properties, resulting in materials with improved shear-thinning behavior, tunable yield stress, and enhanced extensional properties [18].

Die swelling is a flow instability observed during extrusion, where the material expands upon exiting the nozzle due to elastic recovery [19]. The degree of die swelling is influenced by the rheological behavior of the EVP fluid, particularly its elasticity and yield stress, among other factors [20]. These properties are particularly relevant for 3D printing, where the ability to maintain shape fidelity and structural integrity is crucial. The blending of Carbopol and PEO provides a pathway to fine-tune printability. The balance between viscosity and elasticity determines the material's ability to flow through the nozzle while maintaining structural stability post-extrusion [21]. The viscoelastic nature of these blends also contributes to droplet formation in inkjet applications, where controlled detachment and spreading behavior are essential for print quality [22]. By adjusting polymer concentration and molecular weight, material deposition and layer cohesion could be enhanced [23].

The ability to fine-tune the rheological properties of Carbopol-PEO blends by adjusting factors such as polymer concentration, pH, and salt content makes them versatile model fluids for studying and optimizing extrusion-based 3D printing processes. In this study, we investigate Carbopol-PEO blends as model fluids for extrusion-based 3D printing, focusing on the role of their elastoviscoplastic (EVP) properties in shaping post-extrusion flow behavior. Specifically, we examine how viscoelasticity, yield stress, surface tension, and extrusion pressure influence die swelling and flow dynamics upon deposition. A parametric analysis is conducted using the dimensionless Ohnesorge number and the modified Bingham number to assess printability limits and identify regimes where stable filament formation is achieved. Structural insights into the nano-structure of the

blends are obtained using Small Angle X-ray Scattering (SAXS). Finally, we evaluate the effect of die swell on the fidelity of printed structures, providing insights into optimizing material formulations and extrusion conditions for improved printing performance.

2 | Experimental Section

2.1 | Sample Preparation

Carbopol was a homopolymer of acrylic acid cross-linked with polyethers. When neutralized with an aqueous base, due to electrostatic repulsions between carboxylic acid groups, the polymer molecules uncoil, resulting in a tenfold swelling of the particles [12]. Solutions were prepared by dispersing Carbopol 980 NF (Lubrizol, USA) in deionized water and homogenizing using a high torque overhead stirrer attached with a propeller-blade (Heidolph Hei Torque Ultimate 400, Heidolph Elektro GmbH, Germany) at 1200 RPM for 30 min. Subsequently, the acidic solution was neutralized with 18 wt. % NaOH solution [24] and stirred at 2000 RPM for 1h. Polyethylene oxide (Sigma–Aldrich, Meck, USA) ($M_W = 4 \times 10^6$ Da), a polyether compound, was dispersed in deionized (DI) water and stirred until homogenized. Carbopol-PEO blends with concentrations in the range 0.05 to 0.125 wt.% were prepared by mixing the two solutions for 30 min.

2.2 | 3D Printing Setup and Data Analysis

A BIO-X bioprinter (Cellink AB, Gothenburg, Sweden) with a pneumatic print head was used to extrude the blends, using a 3 ml syringe attached to a 22G blunt needle (needle diameter, $D_n = 0.41$ mm), Figure 1a,b. A Dolan-Jenner fiber optic illumination system (Edmund Optics, New Jersey, USA) equipped with a ring light source was placed behind the printhead to illuminate the extrusion area with a non-reflective black background. A Canon EOS 90D DSLR camera (Canon Inc., Tokyo, Japan) with a series of microscopic lenses (LMscope, Austria) installed was used to record videos of the extrusion at 120 frames per second. The prepared blends were carefully poured into the syringe to avoid air entrapment and any remaining entrapped air was released using a vortex mixer. Samples were extruded at pressures (P_{ext}) 100, 150, and 200 kPa and videos were recorded when steady flow was achieved. Frames extracted from the videos were color corrected and processed using a custom MATLAB code to find the width (W_{DS}) and position (distance from the needle outlet, L_{DS}) of the die swell, Figure 1c,d. Experiments were performed in triplicates and W_{DS} was averaged.

The prepared samples were 3D printed using the same setup and pressures. To accommodate cases with high L_{DS} while maintaining an appropriate gap for 3D printing, the needle was positioned at a height equal to D_n. Various print velocities were tested, and the highest velocity that ensured continuous printing ($V_P = 50$ mms^{-1}) was selected to minimize material spread upon deposition on the print bed. The printed lines were photographed and the steady state print width (W_P) was calculated at three different positions and averaged.
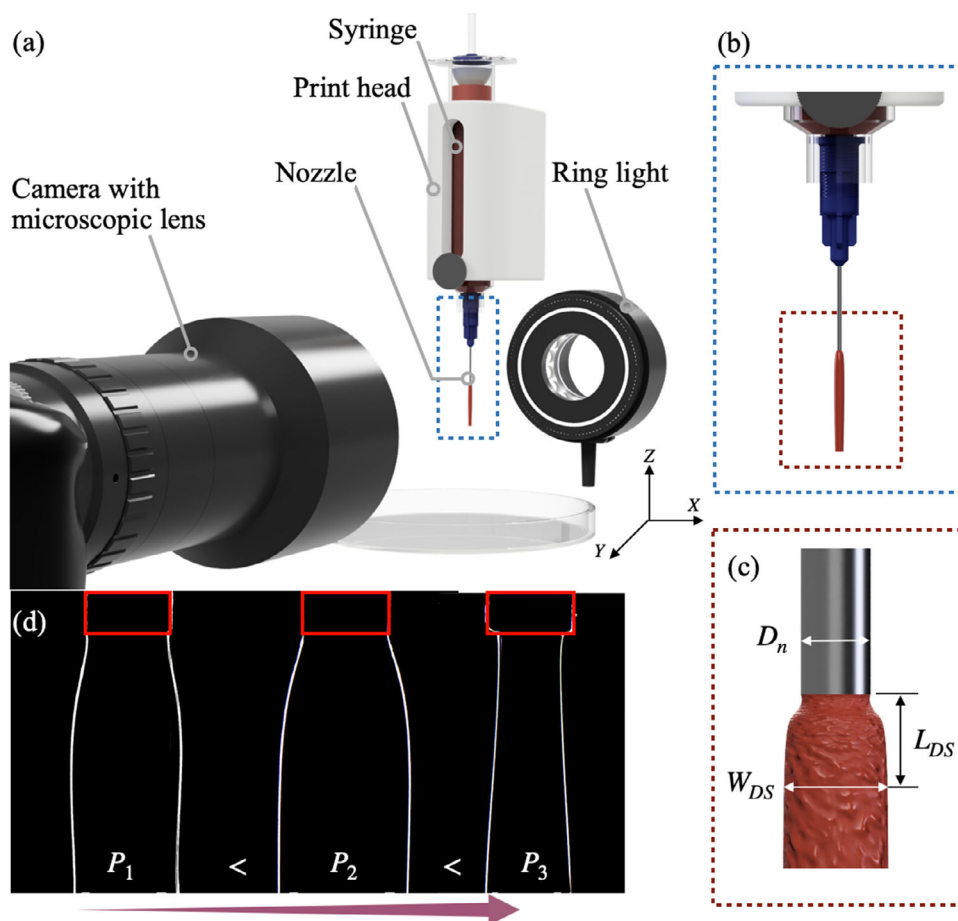
FIGURE 1 | Visualization setup showing a) a 3 ml syringe installed in the pneumatic print head positioned between a ring light and a DSLR camera with microscopic lenses. The syringe is fitted with a (b) needle of diameter, $D_n = 0.41$ mm. c,d) Width and position of the die swell measured with respect to the needle orifice, using custom video post processing script.

2.3 | Characterizations

2.3.1 | Rheology

Steady state shear and oscillatory rheological tests were performed on an Anton Paar MCR702e Space rheometer (Graz, Austria) using profiled bob and cup measuring geometries (CC27/P6) with a gap of 1 mm. Measurements were performed in single motor-transducer configuration with the C-ETD 200/XL accessory to maintain the measuring temperature constant at 23 °C. Rate-controlled steady shear tests were performed at $\dot{\gamma} \in [10^{-3}, 10^2]\,\text{s}^{-1}$ and the steady state shear stress (σ) was measured. Oscillatory shear tests were performed at $\gamma_0 \in [10^{-3}, 10^3]\%$ at a constant angular frequency of 6 rads^{-1} and the dynamic moduli were measured.

2.3.2 | Rheo-SAXS

In situ rheology and small-angle X-ray scattering (Rheo-SAXS) setup, tests and data synchronization were based on our previous study [25]. Rheo-SAXS experiments were performed at the CoSAXS beamline at MAXIV Laboratory, Lund, Sweden. The sample-to-detector (EIGERX 4M) distance was set to 14.8 m at

15 keV energy. The scattering vector range was $q \in (10^{-3}, 8 \times 10^{-1})\,\text{Å}^{-1}$.

Rheo-SAXS experiments were performed on an Anton Paar MCR702 Multidrive rheometer (Anton Paar, Austria) equipped with standard polycarbonate (PC) concentric cylinder (CC) geometry with an inner cylinder radius of 24.5 mm and an outer cup of radius 25 mm. To study the relaxation phenomena, tests were performed in two steps. First, materials were sheared at $\dot{\gamma}_s = 10^3$ s^{-1} for 30 s, followed by relaxation at $\dot{\gamma}_r = 10^{-4}$ s^{-1} for 3000 s. During the tests, X-rays were continuously collected with an exposure time of 0.1 s per frame in the radial position of the CC geometry (1–3 plane).

Scattering data were processed using a Jupyter Notebook-based workflow, originally developed at MAX IV and modified for our dataset. Transmission normalization was applied at the 2D detector level to account for fluctuations in incident beam intensity and exposure time on a frame-by-frame basis. The normalized 2D patterns were then radially integrated to produce 1D $I(q)$ profiles, which were averaged over selected frames. Background scattering from the polycarbonate (PC) geometry filled with water was measured separately, processed in the same way, and then subtracted from the sample curves. The final corrected radially
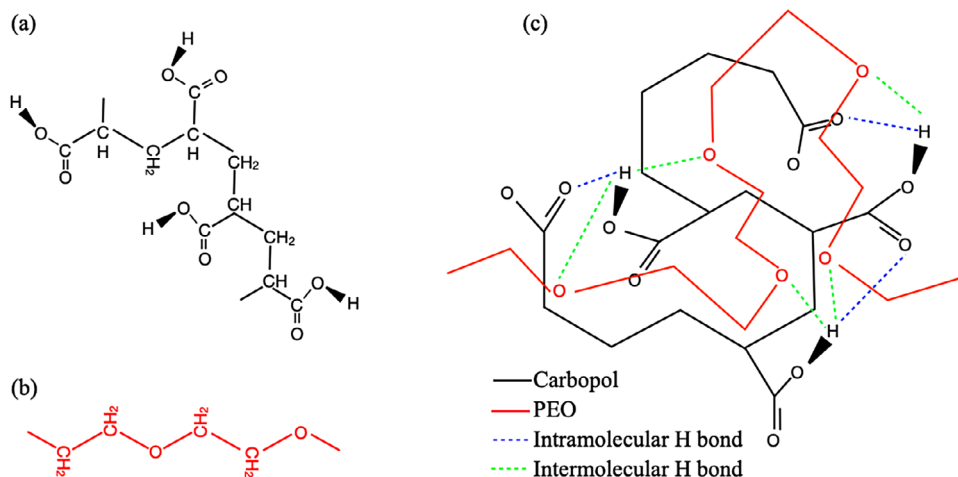
FIGURE 2 | Schematic showing a) Cross-linked Carbopol polymer and b) linear chain PEO molecule. c) Molecular structure of Carbopol/PEO blend, with Carbopol microgel in black and PEO molecule in red. The dotted blue and green lines represent intra and intermolecular hydrogen bonding respectively.

integrated intensities, $I(q)$, were used for further analysis and are expressed as:

$$I(q) = I_{raw}^{norm}(q) - I_b^{norm}(q) \qquad (1)$$

where $I_{raw}^{norm}(q)$ and $I_b^{norm}(q)$ are the normalized and radially integrated intensities of the sample and background, respectively. The normalization factor is computed as:

$$\text{norm} = \frac{I_t - I_{\text{dark},t}}{I_0 - I_{\text{dark},0}} \times \frac{I_{\text{empty},0} - I_{\text{dark},0}}{I_{\text{empty},t} - I_{\text{dark},t}} \times dt \qquad (2)$$

here, I_0 and I_t are the incident and transmitted intensities during the sample measurement; $I_{\text{dark},0}$ and $I_{\text{dark},t}$ are corresponding dark currents; and $I_{\text{empty},0}$, $I_{\text{empty},t}$ are the incident and transmitted intensities measured for the empty PC cell and dt is the exposure time of the sample measurement.

2.3.3 | Surface Tension

The surface tension of the blends was measured with the pendant drop method using a syringe with a needle diameter of 0.718 mm installed on an Attension Theta optical tensiometer (Biolin Scientific, Finland). The surface tension was determined by fitting the Young-Laplace equation on the black and white contour of the droplet captured using a digital camera.

3 | Results and Discussion

Carbopol is a high-molecular-weight acrylic acid-based polymer cross-linked with polyalkenyl ethers or divinyl glycol, Figure 2a. When dispersed in water, cross-linked Carbopol polymer undergoes extensive swelling, expanding its volume up to 1000 times and increasing its diameter nearly tenfold. This swelling results in a mucilage-like dispersion with an acidic pH of approximately 3. However, when the pH exceeds 4–6, the carboxylate groups on the polymer backbone ionize, generating negative charges [14]. This ionization leads to electrostatic repulsion among polymer chains,

further enhancing polymer swelling. The addition of a neutralizing agent, such as sodium hydroxide (NaOH), facilitates this process by promoting ionization, ultimately leading to extensive polymer expansion and gel formation. Unlike linear polymers, cross-linked Carbopol does not dissolve in water; instead, they form a stable gel network due to their crosslinked structure [16].

PEO consists of ethylene oxide monomers which are polymerized into a linear chain, Figure 2b. The hydrogen bonding between PEO ether oxygen and the carboxylic acid group of Carbopol facilitates miscibility of the two materials [16, 26], Figure 2c. Diameter of the swollen Carbopol microgel particle, $\mathcal{O}(1)\mu m$, is several orders of magnitude larger than PEO molecules $\mathcal{O}(10)nm$ [14]. At a critical PEO concentration, C_P^*, PEO changes the effective volume fraction of the particles leading to an increase in viscoelasticity due to enhanced interparticle interactions between the microgel units of Carbopol and the PEO molecules. The critical PEO concentration was calculated from the average molecular weight as, $C_P^* = 1/0.0125(M_V)^{0.78} = 0.056$ wt.%. Therefore, $C_P \geq 0.05$ wt. % has been chosen for this study. In the relaxed state several PEO molecules are attached to the microgel via hydrogen bonding. At a critical Carbopol concentration, C_C^*, yield stress increases as a result of jamming of the system, caused by overlapping of the hypothetical spheres encompassing the polymer chains.

3.1 | Rheology

3.1.1 | Rheology of Reference Compositions

Within the PEO concentration range considered in this study, $C_P \in [0.05, 0.125]$ wt%, the solutions remain in the dilute regime, as evidenced by their viscous dominated linear viscoelastic behavior ($G'' > G'$), Figure 3a. Increasing the concentration in this range has little to no effect on the the dynamic moduli. The flow curve obtained is typical of shear thinning fluids, Figure 3b. Carbopol exhibits viscoelastic characteristics at $C_C = 0.05$ wt. %, with a dominant viscous behavior ($G'' > G'$). Note that at the lowest concentration, Carbopol is weakly elastic and the
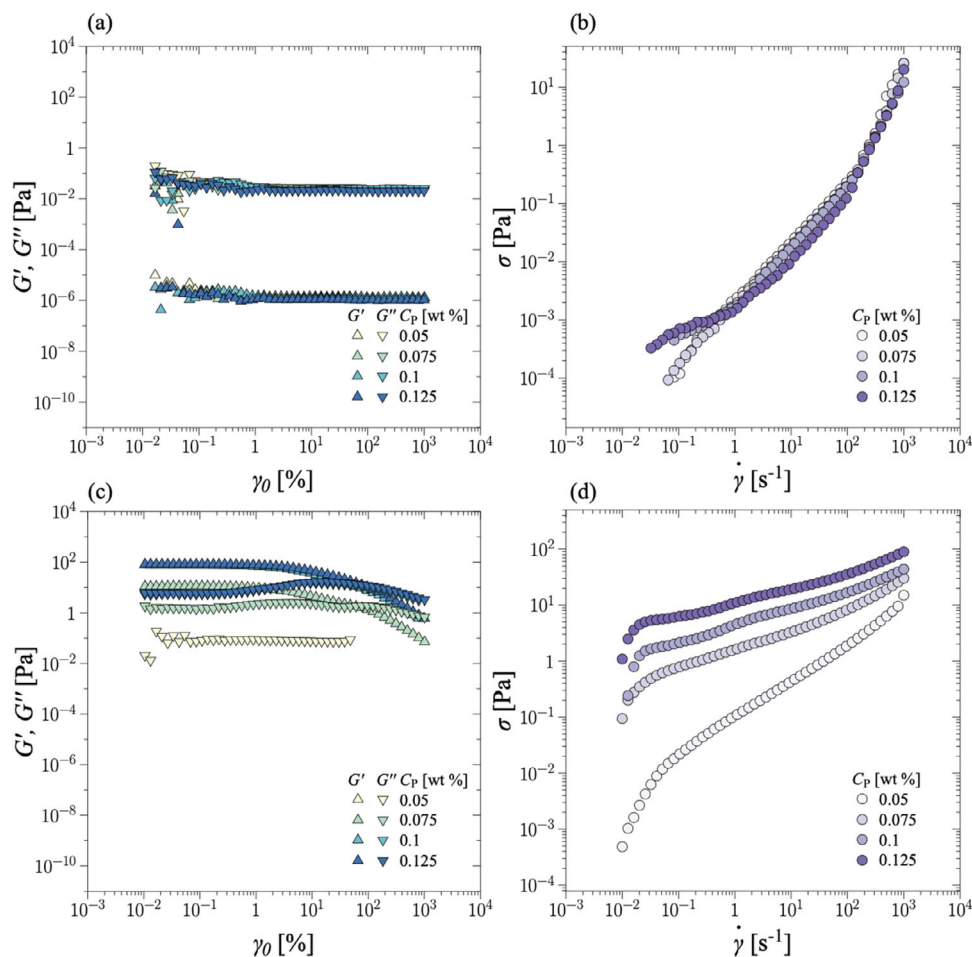
FIGURE 3 | Steady state oscillatory and shear rheological curves at various concentrations of (a), (b) PEO (C_P) and (c),(d) Carbopol (C_C). In subfigures (a) and (c) G' and G'' are represented by upward and downward facing triangles respectively.

storage modulus was not measurable, even with a double gap measuring geometry. Percolation is likely achieved somewhere between $C_C \simeq 0.05$ and 0.075 wt. %, with the formation of a microgel network imparting gel like characteristics to the material ($G' > G''$), and resulting in a steep increase in the dynamic moduli, Figure 3c. Angular frequency sweep tests confirm the viscous dominated behavior of PEO samples and Carbopol (at $C_C = 0.05$ wt. %) across the entire frequency range measured. Frequency sweep curves for the lowest concentration of Carbopol and PEO can be found in the Supporting Information.

The dynamic moduli are independent of the imposed strain amplitude in the linear viscoelastic regime (LVR), at low strain amplitudes. The critical strain, at which material departs from the LVR, decreases with an increase in C_C. After the LVR, G'' shoots up while G' decreases. The weak strain overshoot (WSO) indicates formation of a weak microstructure that resists flow [27]. At high strain amplitudes the structure is destroyed and the polymeric chains align in the flow direction, aiding flow. From a microstructural point of view, weak strain overshoot has been associated to jamming followed by yielding. After the crossover, the dynamic moduli decrease in the LAOS regime, as expected. Carbopol is shear thinning and shows viscoplastic behaviour (yield stress) for $C_C \geq 0.075$ wt. %, in the gel state, Figure 3d. The change in slope of the flow curves at the critical

shear rate $\dot{\gamma}_C \approx 0.1$ s^{-1}, marks the transition from elastic to viscoplastic deformation.

3.1.2 | Rheology of the Blends

All blend compositions considered exhibit gel-like characteristics with $G' > G''$ in LVE, Figure 4a,c,e,g. At $C_C = 0.075$ wt. %, addition of PEO in small quantities ($C_P = 0.05$ wt. %) leads to a large increase in dynamic moduli by one order of magnitude, Figure 4c. The Carbopol microgel network, augmented by PEO, starts to dominate at $C_C = 0.1$ wt. % as evidenced by the presence of a yield stress A further increase in PEO ($C_P \geq 0.075$ wt.%) leads to a slight decrease in the dynamic moduli (Figure 4e,g). The blends exhibit weak strain overshoot at $C_C \geq 0.1$ wt.%, and in dilute blends ($C_C \leq 0.075$ wt.%), an increase in moduli at high strain suggests possible stress induced reorganization and alignment.

The yield stress increased by approximately an order of magnitude when the concentration of Carbopol was increased, Figure 4b,d,f,h. However, increasing C_P also increased the yield stress by a few tens of pascals. This is likely due to increased jamming caused by the intermolecular H-bonding between PEO molecules and Carbopol microgel particles. The steady-state
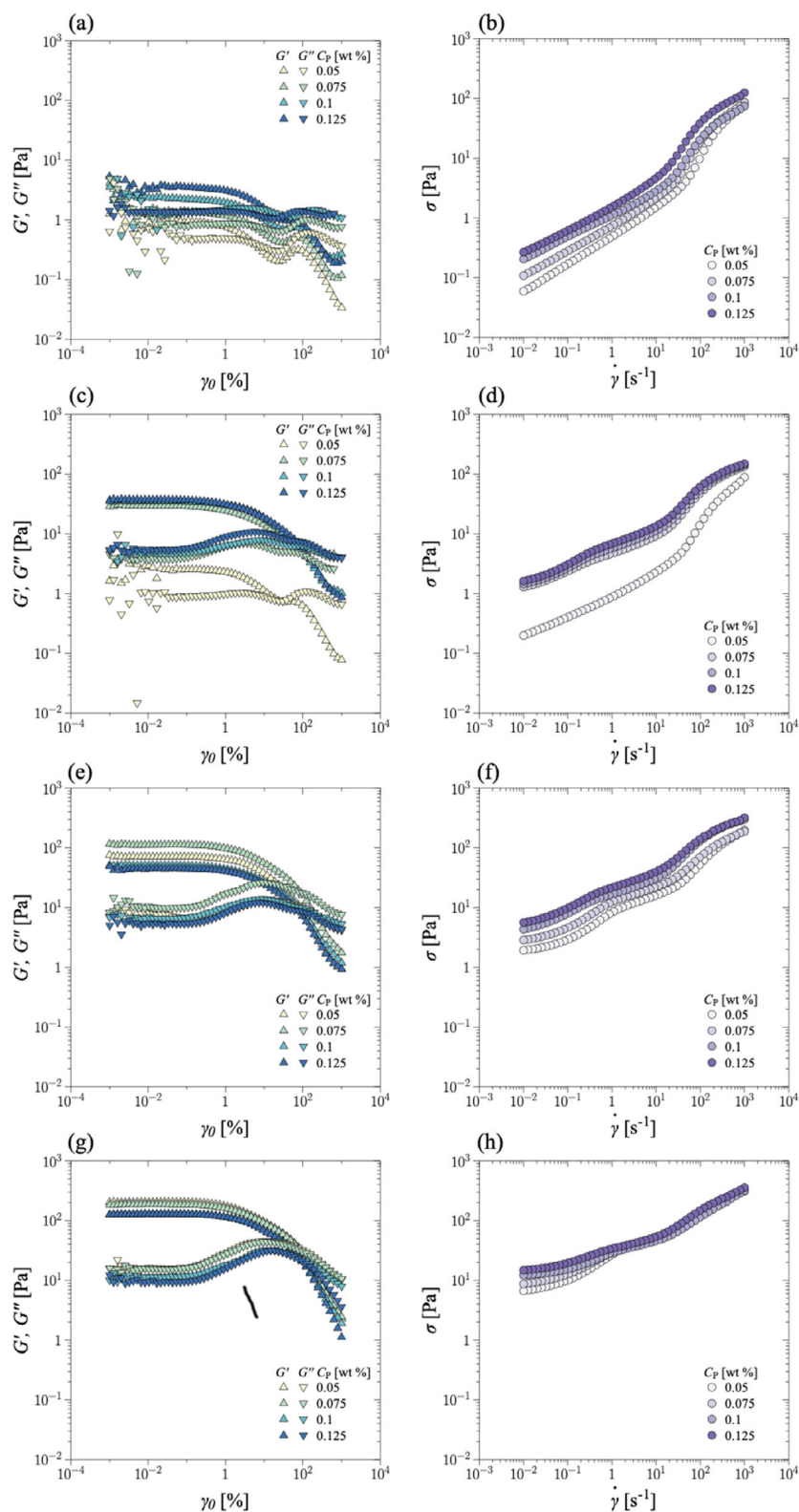
FIGURE 4 | Steady state strain sweep (left) and flow curves (right) at different Carbopol concentrations: a,b) $C_C = 0.05$ wt. %, c,d) $C_C = 0.075$ wt. %, e,f) $C_C = 0.1$ wt. %, and g,h) $C_C = 0.125$ wt. %. Rheological curves were measured at four different PEO concentrations, $C_P \in [0.05, 0.125]$ wt. %. In strain sweep plots, G' and G'' are represented by upward and downward facing triangles respectively.
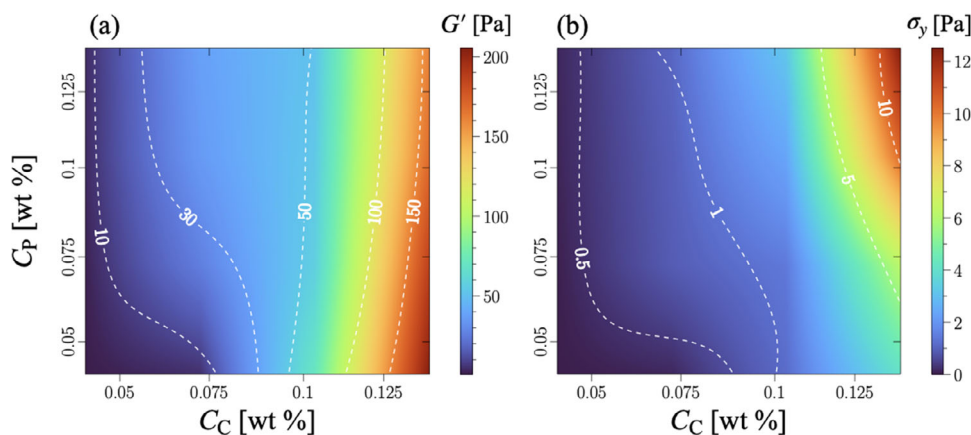
FIGURE 5 | Contours plots displaying the influence of C_C and C_P on the a) storage modulus (G'), and b) yield stress of the blends. Iso-modulus and iso-stress lines are shown in white.

flow curves in Figure 2 were fitted with the Herschel-Bulkley viscoplastic model (see Equation S1, Supporting Information) to obtain the yield stress, consistency index and flow index. The flow curves show a decrease in slope (flow index) at $C_C \geq 0.1$ wt. % indicating an increase in the shear thinning behavior. The flow curves are representative of the material heterogeneity, which results in the flow curve displaying three distinct regions with difference in slope, caused by the complex structural dynamics of the blends under shear conditions. Such behavior has previously been observed for gels with heirarchical structure [28].

The influence of Carbopol and PEO on the elasto-viscoplastic behavior of the blends is summarized in the contour plots of the storage modulus (G') and yield stress (σ_y) in Figure 5a,b, respectively. G' increases significantly as C_C increases and moderately with an increase in C_P, up to a critical Carbopol concentration, $C_C^* = 0.075$ wt. %. Beyond this point, further increasing C_P leads to a slight decrease in G'. Yield stress increases with C_C, however, below the critical concentration (C_C^*) the yield stress is independent of C_P. When $C_C > C_C^*$, yield stress increases with C_P.

3.2 | Die Swelling

The Ohnesorge number (Oh) is a dimensionless number that relates viscous forces to inertial and surface tension forces. $Oh = \eta/\sqrt{\rho \sigma_{ST} D_n}$, where η is the viscosity of the fluid, ρ is the fluid density, σ_{ST} is the surface tension, and D_n is the diameter of the capillary channel, in this case inside the needle. The measured surface tension for the various blends can be found in the Supporting Information. The density of the samples has been approximated from the density of the neat Carbopol solution, from our previous work [29]. To find the average viscosity at the outlet of the needle capillary channel, CFD simulations were performed using the regularized Herschel Bulkley equation to model the rheology of the blends. More information regarding simulation setup and the implemented rheological model can be found in the Supporting Information. Oh was calculated for the blends at three different pressures and plotted against the Reynolds number, $Re = \rho \overline{V_z} D_n / \overline{\eta}$, Figure 6a. Oh decreases with an increase in Re as the points collapse onto a power

law given by $Oh = 3.2 Re^{-0.57}$. An increase in viscosity at high concentrations result in low Re and high Oh. Different regimes can be identified. Although the recommended range of Oh for drop formation (inkjet printing) depends largely on the material rheology, typically $0.07 < Oh < 1$ can be considered optimal [30]. When $Oh \geq 1$, the material is considered too viscous, i.e., droplet break off does not occur (region marked with blue). At $Oh \leq 0.07$, satellite drops form, preventing the extrusion of consistent droplets (region marked with pink). The criterion for the flow to have sufficient kinetic energy for drop formation is given by the Derby criterion, $Re \leq 2/Oh$ (left orange line). Whereas, the onset of splashing of the droplet when it comes in contact with the substrate is given by $OhRe^{5/4} \geq 50$ (right orange line). Therefore, samples with the lowest Carbopol concentration $C_C = 0.05$ wt. % and high PEO concentrations $C_P = 0.1, 0.125$ wt. % are optimal for inkjet printing, at $10^1 < Re < 10^2$ (region marked with orange).

We define a modified Bingham number ($\xi/Bi = \frac{\eta\dot{\gamma}}{\sigma_y} \cdot \frac{G'_{LVR}}{\sigma_y}$), the latter of which gives the ratio of viscoelastic forces to yield stress of the material. Oh varies with the heuristically modified Bi number with a sigmoid relationship shown in Figure 6b. The optimal material response for inkjet printing, from Figure 5a, has predominantly viscoelastic characteristics and negligible yield stress (high ξ/Bi in Figure 5b) which allows for droplet formation, governed by surface tension. An example of this is shown in a snapshot of the extrudate at point (iv), where low Oh, and high Re and ξ/Bi result in a pulsating stream of fluid which breaks off and forms droplets (snapshots in SI). As we increase Oh and decrease Re and ξ/Bi, the material becomes too viscous to allow drop formation, and a continuous stream of fluid starts to form (see snapshots (i) − (iii)). This is achieved at high C_C as the yield stress increases and the surface tension becomes less significant.

When yield stress of the material is considerable, $\sigma_y \geq 1$ Pa & $\xi/Bi \leq 8 \times 10^4$ (corresponding to $C_C = 0.1\%$ and $C_P = 0.075\%$), the flow index n (from Herschel-Bulkley fits to the flow curve, Figure 4) drops from 0.48 to 0.41 indicating an increase in shear thinning behavior as ξ/Bi decreases. Therefore, an increase in extrusion pressure results in a drop in Oh as the viscosity decreases at increasingly high shear. At high ξ/Bi, yield stress and viscosity are low enough to allow viscoelastic and surface
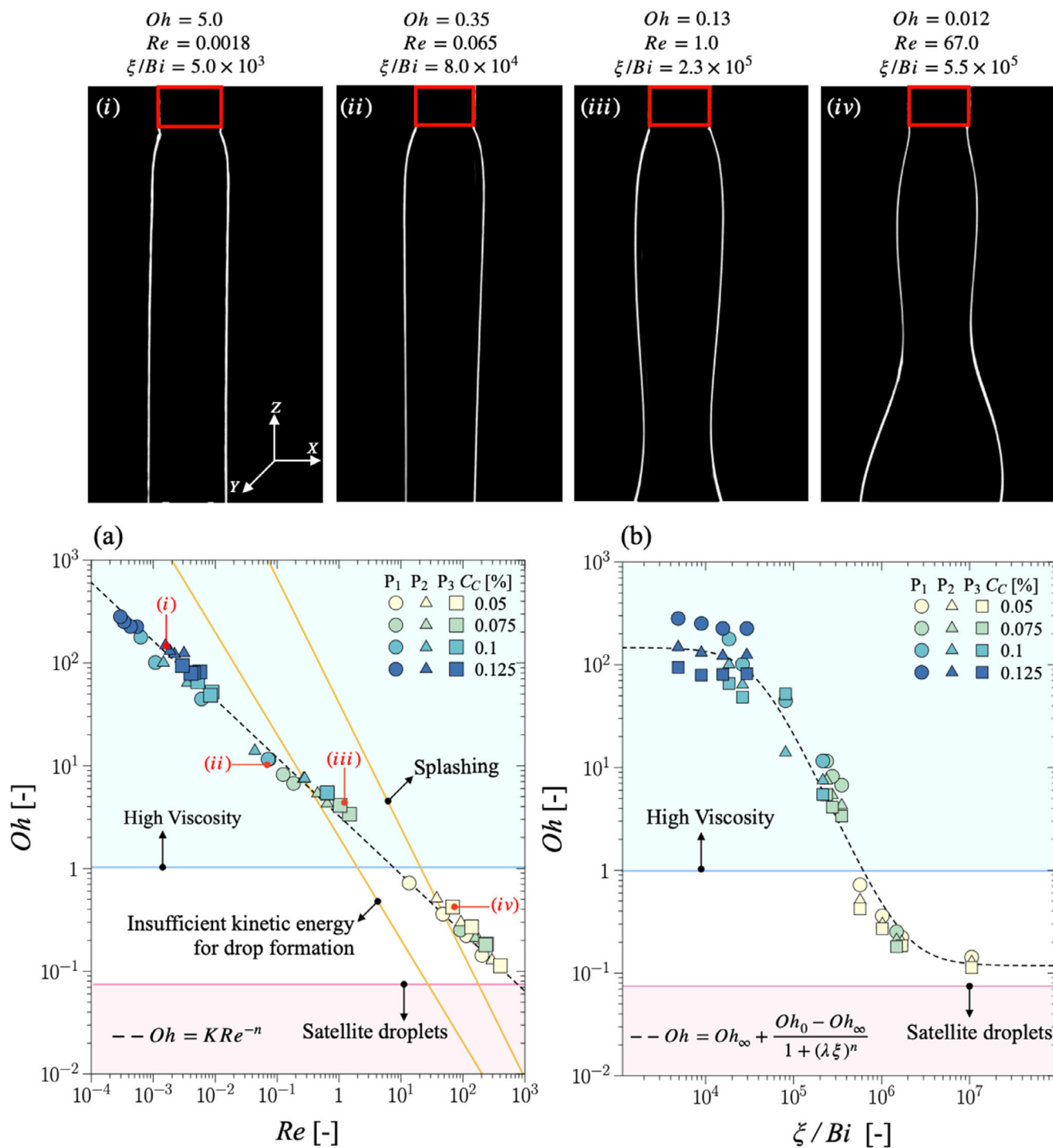
FIGURE 6 | a) Ohnesorge number (Oh) versus Reynolds number (Re) plot showing various flow regimes. Region marked with orange represents the optimal regime for droplet formation. The high viscosity regime (blue region) is suitable for 3D printing. Symbols represent the various concentrations of Carbopol and PEO that were studied at extrusion pressure, $P_{ext} = 100$ (P_1), 150 (P_2) & 200 (P_3) kPa. The dotted line shows the power law relationship between Oh and Re. Snapshots of the die swell showing (i) steady stream with die swell when viscosity is high, (ii) steady stream with downstream decreasing width at moderate viscosity, (iii) unsteady stream and onset of drop formation downstream, and (iv) unsteady pulsating stream and drop formation at low viscosity. b) Oh as a function of the modified Bingham number, ξ/Bi. Dotted line represents a sigmoidal function fitted to the data points.
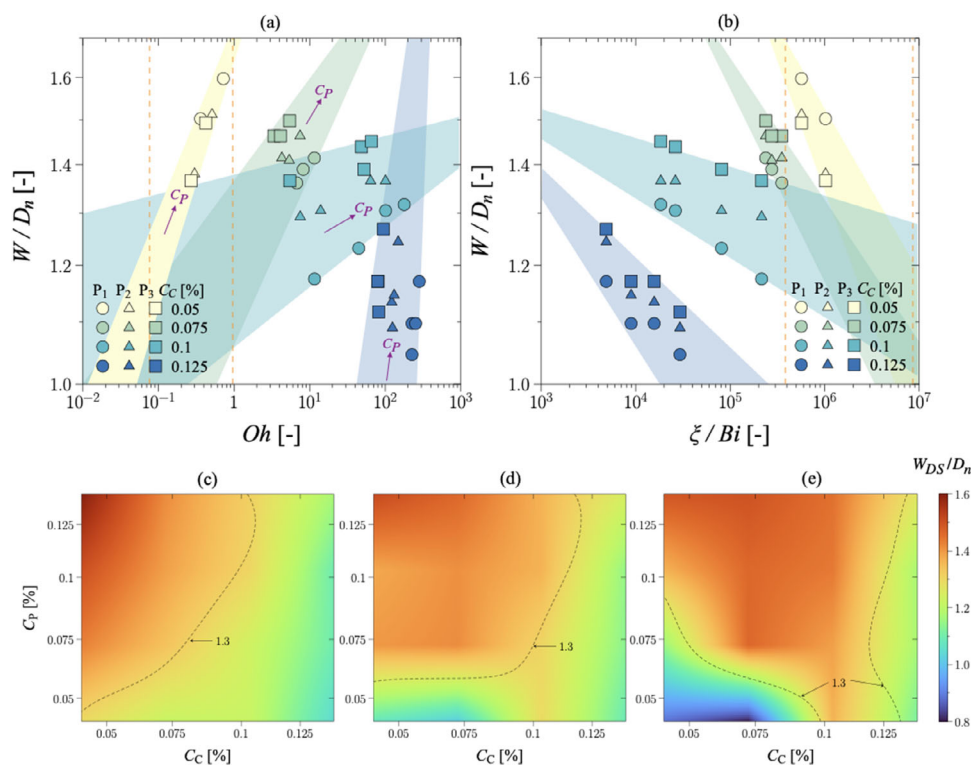
FIGURE 7 | Variation of die swell ratio as a function of the a) Ohnesorge number (Oh), and b) modified Bingham number (ξ/Bi) for the different blends studied, at extrusion pressure, $P_{ext} = 100\,(P_1)$, $150\,(P_2)$ & $200\,(P_3)$ kPa. Dotted lines mark the region where droplet formation occurs downstream. Die swell ratio as a function of Carbopol (C_C) and PEO (C_P) concentrations at three different extrusion pressures, P_{ext} = c) 100, d) 150 and e) 200 kPa. Black dotted iso-width lines mark the high die swell region.

tension forces to take over. The three dimensionless numbers Oh, Re and ξ/Bi, can be used for *apriori* estimation of the suitability of an EVP for inkjet and 3D printing. From Figure 6b, the sigmoid function can be used to approximate Oh from the rheological functions of the fluid, and calculate Re and the extrusion velocity from Figure 6a. Furthermore, the optimal extrusion pressure (P_{ext}) can be calculated to achieve desired post-extrusion flow behavior.

The die swell ratio, W_{DS}/D_n, defined as the width of the die swell, W_{DS} (Figure 1c), with respect to the diameter of the orifice, was calculated and plotted as a function of Oh (Figure 7a) and ξ/Bi (Figure 7b). Die swell increases with a decrease in Oh. At high Oh, the high viscosity of the blends hinders the relaxation of the polymeric chains as the material exits the orifice. However, die swell increases with the extrusion pressure in this regime. In such a scenario, polymeric chains would be expected to elongate and align due to high stresses close to the wall of the needle at high pressures. However, due to the combination of Carbopol (microgel) and PEO polymer chains, confinement effects induced by the deformable Carbopol-PEO network play a major role in die swell. Instead of die swell being primarily driven by the stretching and relaxation of PEO polymer chains, the Carbopol-PEO network itself deforms and expands as it exits the orifice. Supporting this, rheological measurements combined with small-angle X-ray scattering did not detect shear-induced orientation in the blends (data not shown), further indicating that network deformation, rather than polymer chain orientation, governs die swell at high Oh. Upon exiting the needle orifice, the pressure drops to atmospheric pressure and the polymeric

chains partially relax and curl up due to elastic recovery. At low Oh, yield stress is negligible and the polymeric chains fully relax upon exiting the orifice. Therefore the die swell is independent of the extrusion pressure. As Oh increases and viscosity becomes sufficiently high ($Oh > 1$), higher extrusion pressures are required to induce polymer conformational changes and subsequent relaxation, resulting in an increase in die swell with extrusion pressure. At $Oh \approx 50$, the viscosity of the material is high enough and the extrusion pressure is insufficient for material relaxation before breakup of the extruded stream of fluid. At the lowest concentrations, $Oh < 0.07$, a steady stream of fluid can not be achieved and high surface tension results in droplet formation. Snapshots of the extrudate during droplet formation can be found in the Supporting Information. Die swell increases significantly with an increase in C_P. When $C_C \leq C_C^*$, the linear polymeric chains of PEO undergo relaxation and are the primary contributors of die swell. Whereas the microgel concentration is insufficient to induce significant intermolecular interactions. Increasing the concentration of Carbopol beyond the critical concentration, $C_C > C_C^*$, induces jamming due to increased interactions between the microgel particles, causing the formation larger aggregates. This prevents complete relaxation of the PEO molecules and decreases die swell. Die swell decreases at low ξ/Bi, where the yield stress of the material is high. For a constant ξ/Bi, die swell can be reduced by decreasing the extrusion pressure.

Figure 7c–e shows the die swell ratio as a function of Carbopol (C_C) and PEO (C_P) concentrations at three different extrusion pressures, $P_{ext} = 100$, 150, and 200 kPa. At low C_C, die swell
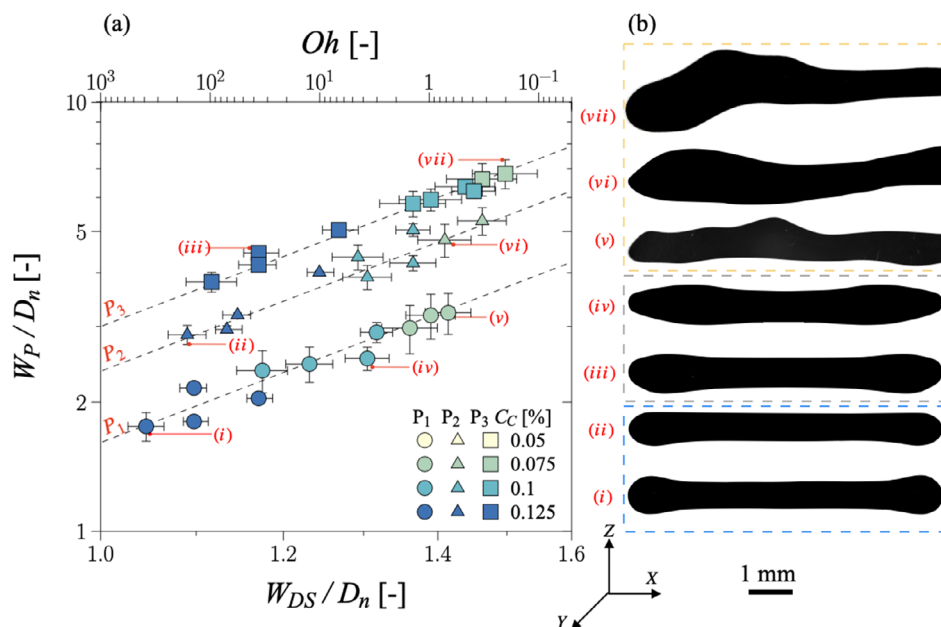
FIGURE 8 | a) Variation of the normalized print width (W_P/D_n) as a function of the die swell ratio (W_{DS}/D_n) and Oh at three extrusion pressures represented by isobaric black lines. b) Snapshots of the printed samples showing, $(i) - (ii)$ optimal print quality at $Oh > 10^2$, $(ii) - (iv)$ onset of material spreading at moderately high Oh ($1 < Oh < 10^2$), and $(v) - (vii)$ poor print quality with high spread at $Oh < 1$.

increases with an increase in C_P and the extrudate swells up to 1.6 times the orifice diameter at $C_P = 0.125$ wt. %. At low C_C, yield stress is negligible and the die swelling is primarily governed by viscoelasticity of the material. As C_C increases, jamming of the structure hinders relaxation and results in a decrease in die swell. Iso-width lines corresponding to a 30% die swell were selected in an ad hoc manner to highlight regions of high die swell. Based on this criteria, die swell is moderately low at $C_C = 0.1$ wt. %, Figure 7c. However, increasing the extrusion pressure promotes stretching and alignment of the polymer chains, resulting in increased relaxation after exiting the orifice. This leads to an increase in die swell even at high C_C, Figure 7d,e. We note that the normal stresses have a significant influence on the die swelling phenomenon. However, determining N_1 and N_2 in such flow conditions can be more challenging without special methods [31, 32].

3.3 | 3D Printing

Carbopol-PEO blends were 3D printed and the mean steady state print width was determined. At the lowest Carbopol concentration ($C_C = 0.05$ wt. %), the material can not be 3D printed due to negligible yield stress. At $C_C = 0.075$ wt. % the blend is semi dilute. However, addition of PEO in low quantities ($C_P = 0.05$ wt. %), increases the water content and dilutes the the system, making it unsuitable for 3D printing, i.e., steady and uniform print can not be achieved for this sample. Especially at high P_{ext}, the material spread post-deposition is as high as 15 times the orifice diameter. These data points have been excluded from the plot in Figure 8. However, high surface tension at such low concentrations allows droplet deposition, appropriate for inkjet printing. Figure 8 shows the variation in width of the 3D printed line as a function of die swell ratio, for the printable samples. Note that an additional axis on the top (in log-scale) shows the variation of Oh. Ideally the printed strand width should be slightly

higher than the nozzle diameter to allow fusion between printed layers due to slight overlap [33]. However, high print width due to excessive spreading is undesirable. For a reasonably high gap between the needle outlet and the print bed, an increase in print width is a result of die swelling. The rheology of the material dictates the extent of spread of the material upon deposition for the given print settings, P_{ext} and V_{Print}. Print width scales up linearly with the die swell ratio. When die swell is low (high Oh and low ξ/Bi), spreading of the material decreases with an increase in C_C and C_P. It was observed that die swell, and therefore the elasto-viscoplastic properties, strongly influence the print width as a 60% increase in die swell can result in up to 200% increase in material spread upon deposition, at low P_{ext}. At high P_{ext}, material spread increases by up to 6–7 times the orifice diameter. Snapshots of the printed lines at points $(i) - (vii)$ in Figure 8a are shown in Figure 8b. Three distinct print regimes can be identified: optimal print at high Oh ($> 10^2$), onset of spreading at moderately high Oh ($1 < Oh < 10^2$), and poor print quality with high spread at $Oh < 1$.

3.4 | Structural Insights Into the Blend's Relaxation Phenomena

While rheological and flow measurements provide a continuum-level perspective on die swelling, uncovering the underlying structural interactions between Carbopol microgels and PEO is crucial for understanding post-extrusion swelling behavior. To investigate these structural features, Rheo-SAXS experiments were conducted on selected neat and blended samples. The Guinier plot, $\ln(I)$ vs. q^2, shown in Figure S4 (Supporting Information) was used to approximate an effective radius of gyration (R_g), a measure of the spatial distribution of scattering elements relative to the center of mass, based on Equation (3). We use the term 'effective', because R_g has distinct physical
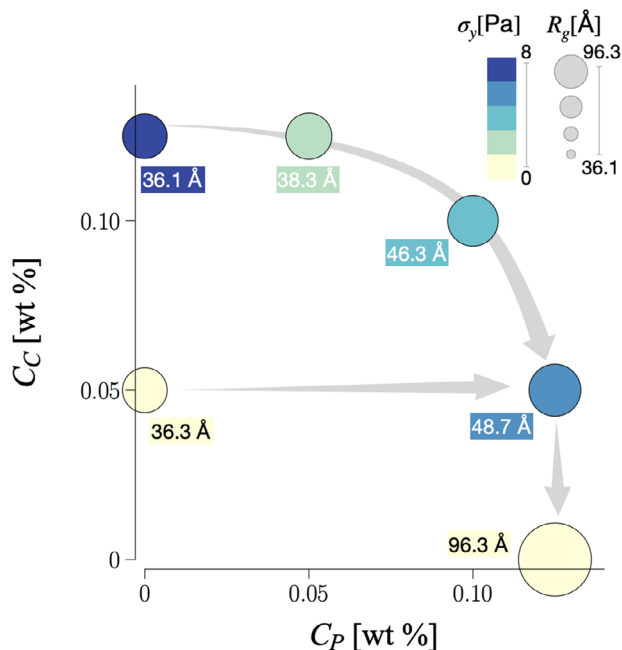
FIGURE 9 | Figure showing the variation of parameter R_g in Equation 3 at different Carbopol and PEO concentrations. R_g increases with the size of the symbols and the colors represent the yield stress of the sample. The labels highlight R_g. We note that depending on the system, R_g can refer to a radius of gyration (PEO), a mesh size (Carbopol) or a correlation length (blends).

interpretation depending on the system studied. It should reflect the radius of gyration of PEO molecules for low concentrations; a characteristic legthscale of the internal microgel structure (mesh size) for Carbopol; and a correlation length for the blends, representing the average size over which spatial density fluctuations in the gel network are correlated. The analysis was performed on intensity curves averaged over the last ten frames of the Rheo-SAXS experiment, meaning it corresponds to the end of the relaxation step. The resulting R_g values are plotted as a function of of(C_C) and (C_P) in Figure 9, and tabulated in Table S2 Supporting Information.

$$\ln(I) = -\frac{R_g^2}{3} \cdot q^2 + \ln(I_0) \tag{3}$$

In neat PEO solutions, R_g corresponds to the coil size of individual polymer chains in the limit of low concentrations. Otherwise, it could reflect larger domains formed by entangled chains. For Carbopol, as the mesh size is determined by the swelling of the microgel, a constant mesh size (R_g) is recorded with increasing C_C. We note also that for low concentrations the scattered signal was comparatively low. Thus the striking increase in yield stress with increasing C_C is attributed to microgel crowding.

In the case of the blends, under shear conditions, a level of orientation in the flow direction would be expected. However, we note that no anisotropy was detected in the SAXS patterns. The presence of die swelling, suggests that there is a substantial relaxation present, due to the presence of PEO. However, confinement effects could hinder PEO chains to orient in the flow direction. As the material relaxes upon the cessation of shear, which here we could consider as representative of the

die exit region, the increase in yield stress suggests a structural reorganization. Interestingly, at low C_C, even small additions of PEO significantly increase the correlation length (R_g). This can be assigned primarily to the hydrogen bonding between PEO chains and the carboxylic acid groups on the microgel [34]. At high C_C, the addition of low concentrations of PEO disrupts this jamming, as flexible PEO chains would mediate microgel-microgel interactions, resulting in a decrease in yield stress. Conversely, when PEO is added in larger amounts, jamming re-emerges marked by an increase in yield stress and correlation length (R_g). Among the samples tested, the blend of $C_C = 0.05$ and $C_P = 0.125$ show the highest correlation length, as well as die swelling (see also Figure 7), suggesting that die swell scales proportionally with the correlation length. Thus, the correlation length could be related to average distances between the microgels as they are separated by PEO chains. Conversely, the re-emerging of jamming could suggest a certain level of phase separation, whereby more microgel-rich domains form a network responsible for the increase in yield stress, while more PEO-rich domains would contribute to relaxation phenomena. A higher correlation length could therefore mean more PEO chains away from the microgel surface allowing for greater mobility under shear and thus greater relaxation.

4 | Conclusion

This study investigated the elasto-viscoplastic (EVP) properties of Carbopol-PEO blends and their effect on extrusion-based 3D printing. The material transitions from a viscous-dominated state ($G'' > G'$) at low Carbopol concentrations ($C_C = 0.05$ wt. %) to a gel-like structure ($G' > G''$) at higher concentrations ($C_C \geq 0.075$ wt. %), with yield stress increasing from 0.1 to 7.8 Pa. The addition of PEO enhances viscoelasticity at low C_C, increasing relaxation effects and die swelling, whereas at higher C_C, the microgel network dominates, suppressing die swelling due to jamming effects. The flow index (n) decreases from 0.48 to 0.41 with increasing C_C, highlighting increased shear-thinning behavior. Die swelling and deposition behavior are governed by the Ohnesorge number (Oh) and the modified Bingham number (ξ/Bi). At low C_C (0.05 wt. %) and high C_P (0.125 wt. %), die swell reaches up to 1.6 times the nozzle diameter ($D_n = 0.41$ mm), whereas at high C_C (≥ 0.1 wt. %), jamming limits it to $1.2D_n$. A direct relationship between die swell and material spreading was observed, where a 60% increase in die swell resulted in up to 200% more spreading at $P_{ext} = 100$ kPa and up to 600% at $P_{ext} = 200$ kPa. Three printability regimes were identified: 1) optimal printability at $Oh > 10^2$ and $\xi/Bi \leq 8 \times 10^4$, ensuring high shape fidelity with minimal die swelling, 2) moderate spreading at $1 < Oh < 10^2$, and 3) poor printability at $Oh < 1$, where excessive spreading and instability lead to unprintable conditions. These findings provide a framework for optimizing EVP material formulations and extrusion conditions, allowing for controlled post-extrusion flow dynamics and improved precision in 3D printing applications. Rheo-SAXS measurements revealed that die swelling correlates strongly with nanoscale lengthscales (SAXS), quantified by a correlation length, which increases significantly upon PEO addition at low C_C. These structural insights complement the rheological findings and emphasize the role of molecular-scale interactions in governing macroscopic extrusion behavior.

Conflicts of Interest

The authors declare no conflicts of interest.

Data Availability Statement

The data that support the findings of this study are available from the corresponding author upon reasonable request.

Conflict of Interest

The authors declare no conflict of interest.

1. J. M. Richardot, S. Kim, and S. Jung, "Evaluating Inkjet Printability of Viscoelastic Ink Through Deborah Number Analysis," *Physics of Fluids* 37, no. 2 (2025).

2. M. S. Abdelgawad, S. J. Haward, A. Q. Shen, and M. E. Rosti, "From Yield Stress to Elastic Instabilities: Tuning the Extensional Behavior of Elastoviscoplastic Fluids," *PNAS nexus* 3, no. 6 (2024): 227.

3. M. T. Mollah, R. Comminal, M. P. Serdeczny, B. Šeta, and J. Spangenberg, "Computational Analysis of Yield Stress Buildup and Stability of Deposited Layers in Material Extrusion Additive Manufacturing," *Additive Manufacturing* 71 (2023): 103605.

4. S. Tuladhar, S. Clark, and A. Habib, "Tuning Shear Thinning Factors of 3D Bio-Printable Hydrogels Using Short Fiber," *Materials* 16, no. 2 (2023): 572.

5. G. Giménez-Ribes, L. M. Sagis, and M. Habibi, "Interfacial Viscoelasticity and Aging Effect on Droplet Formation and Breakup," *Food Hydrocolloids* 103 (2020): 105616.

6. M. Mucha, "Polymer as an Important Component of Blends and Composites With Liquid Crystals," *Progress in polymer science* 28, no. 5 (2003): 837–873.

7. M. M. El Sayed, "Production of Polymer Hydrogel Composites and Their Applications," *Journal of Polymers and the Environment* 31, no. 7 (2023): 2855–2879.

8. A. E. Blok, D. P. Bolhuis, L. N. Arnaudov, K. P. Velikov, and M. Stieger, "Influence of Thickeners (microfibrillated Cellulose, Starch, Xanthan Gum) on Rheological, Tribological and Sensory Properties of Low-Fat Mayonnaises," *Food Hydrocolloids* 136 (2023): 108242.

9. D. Krishna, M. Sankar, P. Sarma, and E. Samundeshwari, "Copper Nanoparticles Loaded Gelatin/Polyvinyl Alcohol/Guar Gum-Based 3D Printable Multimaterial Hydrogel For Tissue Engineering Applications," *International journal of biological macromolecules* 276 (2024): 133866.

10. Q. Zeng, S. Wan, S. Yang, et al., "Super Stretchability, Strong Adhesion, Flexible Sensor Based on Fe3+ Dynamic Coordination Sodium Alginate/Polyacrylamide Dual-Network Hydrogel," *Colloids and Surfaces A: Physicochemical and Engineering Aspects* 652 (2022): 129733.

11. Y. Yue, X. Wang, Q. Wu, J. Han, and J. Jiang, "Assembly of Polyacrylamide-Sodium Alginate-Based Organic-Inorganic Hydrogel With Mechanical and Adsorption Properties," *Polymers* 11, no. 8 (2019): 1239.

12. Z. Jaworski, T. Spychaj, A. Story, and G. Story, "Carbomer Microgels as Model Yield-Stress Fluids," *Reviews in Chemical Engineering* 38, no. 7 (2022): 881–919.

13. J. Y. Kim, J. Y. Song, E. J. Lee, and S. K. Park, "Rheological Properties and Microstructures of Carbopol Gel Network System," *Colloid and Polymer Science* 281, no. 7 (2003): 614–623.

14. S. Om, K. Amol, "Carbomer: A Comprehensive Review," *Inventi Rapid: Pharm Tech* 2016, no. 1 (2015): 1–8.

15. M. Y. Danny, G. L. Amidon, N. D. Weiner, and A. H. Goldberg, "Viscoelastic Properties of Poly (Ethylene Oxide) Solution," *Journal of pharmaceutical sciences* 83, no. 10 (1994): 1443–1449.

16. Y. Kumar and U. Natarajan, "Structure of Interpolymer Complex Between Poly (Acrylic Acid) and Poly (Ethylene Oxide) in Aqueous Salt Solution: a Molecular Dynamics Simulation Study," *Molecular Simulation* 49, no. 8 (2023): 743–757.

17. L. A. Kanis, F. C. Viel, J. S. Crespo, J. R. Bertolino, A. T. Pires, and V. Soldi, "Study of Poly (Ethylene Oxide)/Carbopol Blends Through Thermal Analysis and Infrared Spectroscopy," *Polymer* 41, no. 9 (2000): 3303–3309.

18. S. Sen, R. R. Fernandes, and R. H. Ewoldt, "Soft Glassy Materials With Tunable Extensibility," *Soft Matter* 20, no. 1 (2024): 212–223.

19. R. Tanner, "A Theory of Die-Swell," *Journal of Polymer Science Part A-2: Polymer Physics* 8, no. 12 (1970): 2067–2078.

20. A. Al-Muslimawi, H. Tamaddon-Jahromi, and M. Webster, "Simulation of Viscoelastic and Viscoelastoplastic Die-Swell Flows," *Journal of Non-Newtonian Fluid Mechanics* 191 (2013): 45–56.

21. H. Zhang, F. Ye, F. Chen, W. Yuan, and W. Yan, "Numerical Investigation on the Viscoelastic Polymer Flow in Material Extrusion Additive Manufacturing," *Additive Manufacturing* 81 (2024): 103992.

22. Y. Guo, H. S. Patanwala, B. Bognet, and A. W. Ma, "Inkjet and Inkjet-Based 3D Printing: Connecting Fluid Properties and Printing Performance," *Rapid Prototyping Journal* 23, no. 3 (2017): 562–576.

23. J. Borges and J. F. Mano, "Molecular Interactions Driving the Layer-by-Layer Assembly of Multilayers," *Chemical reviews* 114, no. 18 (2014): 8883–8942.

24. R. P. Varges, C. M. Costa, B. S. Fonseca, M. F. Naccache, and d. P. R. Souza Mendes, "Rheological Characterization of Carbopol® Dispersions in Water and in Water/Glycerol Solutions," *Fluids* 4, no. 1 (2019): 3.

25. R. Ghanbari, A. Terry, S. Wojno, et al., "Propagation of Orientation Across Lengthscales in Sheared Self-Assembling Hierarchical Suspensions via Rheo-PLI-SAXS," *Advanced Science* 12, no. 7 (2025): 2410920.

26. K. Pielichowska, S.Głowinkowski, J. Lekki, D. Biniaś, K. Pielichowski, and J. Jenczyk, "PEO/Fatty Acid Blends For Thermal Energy Storage Materials. Structural/Morphological Features and Hydrogen Interactions," *European Polymer Journal* 44, no. 10 (2008): 3344–3360.

27. J. Li, H. Ma, Y. Li, Z. Yang, G. He, and B. Wang, "The Micromorphology and Large Amplitude Oscillatory Shear Behaviors of Hydrocarbon Gel Fuels Filled With Fumed Silica and Aluminium Sub-Microparticles," *Colloids and Surfaces A: Physicochemical and Engineering Aspects* 654 (2022): 130013.

28. S. Wojno, M. Fazilati, T. Nypelö, G. Westman, and R. Kádár, "Phase Transitions of Cellulose Nanocrystal Suspensions From Nonlinear Oscillatory Shear," *Cellulose* 29, no. 7 (2022): 3655–3673.

29. K. Amini, A. A. Mishra, A. K. Sivakumar, et al., "Scaling Laws For Near-Wall Flows of Thixo-Elasto-Viscoplastic Fluids in a Millifluidic Channel," *Physics of Fluids* 36, no. 2 (2024).

30. Y. J. Han, D. Y. Kim, K. An, K. T. Kang, B. K. Ju, and K. H. Cho, "Sequential Improvement From Cosolvents Ink Formulation to Vacuum Annealing For Ink-Jet Printed Quantum-Dot Light-Emitting Diodes," *Materials* 13, no. 21 (2020): 4754.

31. I. F. Naue, R. Kádár, and M. Wilhelm, "A New High Sensitivity System to Detect Instabilities During the Extrusion of Polymer Melts," *Macromolecular Materials and Engineering* 300, no. 11 (2015): 1141–1152.

32. R. Kádár, I. F. Naue, and M. Wilhelm, "First Normal Stress Difference and in-Situ Spectral Dynamics in a High Sensitivity Extrusion Die For Capillary Rheometry Via the hole Effect'," *Polymer* 104 (2016): 193–203.

33. A. A. Mishra, A. Momin, M. Strano, and K. Rane, "Implementation of Viscosity and Density Models For Improved Numerical Analysis of Melt Flow Dynamics in the Nozzle During Extrusion-Based Additive Manufacturing," *Progress in Additive Manufacturing* (2022): 1–14.

34. N. Doungsong, *Synthesis and Characterization of Poly (Acrylic Acid) Based Microgels For Formulation Applications.* PhD thesis. (University of Bristol, 2018).

Supporting Information

Additional supporting information can be found online in the Supporting Information section.

Supporting File 1: marc202500249-sup-0001-SuppMat.pdf.